Magnetic Core−Shell Fe_3O_4@Ag Nanoparticles Coated Carbon Paste Interface for Studies of Carcinoembryonic Antigen in Clinical Immunoassay

Dianping Tang, Ruo Yuan,* and Yaqin Chai

Key Laboratory of Analytical Chemistry (Chongqing), College of Chemistry and Chemical Engineering, Southwest University, Chongqing 400700, P. R. China

Received: February 14, 2006; In Final Form: April 6, 2006

This study demonstrates a novel approach toward development of advanced immunosensors based on chemically functionalized core−shell Fe_3O_4@Ag magnetic nanoparticles, and the preparation, characterization, and measurement of relevant properties of the immunosensor useful for the detection of carcinoembryonic antigen (CEA) in clinical immunoassay. The immunosensor based on the combination of a magnetic nanocore and an Ag metallic shell shows good adsorption properties for the attachment of the CEA antibody selective to CEA. The core−shell nanostructure presents good magnetic properties to facilitate and modulate the way it was integrated into a carbon paste. Under optimal conditions, the resulting composite presents good electrochemical response for the detection of CEA, and allows detection of CEA at a concentration as low as 0.5 ng·mL^{-1}. Importantly, the proposed methodology could be extended to the detection of other antigens or biocompounds.

1. Introduction

Carcinoembryonic antigen (CEA), a kind of glycoprotein with a molecular mass of about 200 kDa found in colorectal carcinomas, is one of the most widely used tumor makers responsible for clinical diagnosis of colorectal, pancreatic, gastric, and cervical carcinomas.[1−3] Thus, the determination of CEA level is very useful to clinical tumor diagnoses. Meanwhile, the CEA level in serum is also related to the state of the tumor, so it can be directly used for evaluating curative effect, judging recrudescence or metastasis as a marker. This study proposed a novel approach toward the detection of CEA in humans and investigated electrochemically the effects of exogenous factors on the performance of the immunoassay system.

In immunoassay systems, biomolecular immobilization is vital in successful development of an immunosensor,[4] and the present immobilization methods are mainly based on adsorption, sandwich, entrapment, covalent binding, or cross-linking technique.[5−12] A basic limitation of passive trapping or adsorption is the instability of proteins immobilization during continuous use.[13] A major limitation of the entrapment technique is the additional diffusion barrier resulting from the entrapped materials, which can be minimized by increasing the porosity of the matrix.[14−16] One of the problems commonly associated with covalent binding is the decrease of protein bioactivity when the proteins are exposed to reactive groups and harsh reaction conditions.[13] In the present paper, we used the physical characteristics of magnetic iron oxide nanoparticles and the good biocompatibility of colloidal Ag nanoparticles to construct a nontoxic biomimetic interface for immobilization of CEA antibody on a Nafion-modified carbon paste electrode surface, which provided an environment similar to a native system and allowed more freedom in orientation of the biomolecules,[17] thus efficiently retaining the activity of proteins and preventing protein leakage from the electrode interface.

Since metallic core−shell types of iron oxide nanoparticles, i.e., owing to inner iron oxide core with an outer metallic shell of inorganic materials such as silica, gold, or gadolinium, not only provided the stability to the nanoparticles in solution but also helped in binding the various biological ligands at the nanoparticle surface for various biomedical applications, the core−shell nanoparticles have been extensively used as a matrix and cytochemical label for the immobilization and study of macromolecules such as drugs, proteins, enzymes, antibodies, and nucleotides and organ, tissue, tumor in hyperthermia.[18−20] Recently, several authors have reported on the magnetic iron or iron oxide nanoparticles coated with Au,[21] gadolinium,[22] and silica.[23−25] In contrast with gold colloids, colloidal Ag nanoparticles have several advantages as follows: (i) Ag nanoparticles exhibit a surface plasmon band between ∼390 and 420 nm that is a spectral regime that is distinct from that of Au (510−560 nm)[26] and (ii) the extinction coefficient of the surface plasmon band for an Ag particle is approximately 4 times as large as that for an Au particle of the same size.[27] Therefore, a major advance would be to propose a method for designing particles with the physical properties of an Ag nanoparticle composition but with the surface chemistry of iron oxide.

This work proposes a novel approach for these purposes. [For this study, we used CEA antigen and CEA antibody as a model.] Anti-CEA molecules were initially absorbed on the core−shell Fe_3O_4@Ag magnetic nanoparticle surface, and then attached to the Nafion-modified carbon paste interface with the aid of a permanent magnet. The performance and factors influencing the sensor's performance were proposed. The resulting immunoassay system exhibited an excellent electrochemical behavior for the detection of CEA. Furthermore, the developed immunoassay methodology was rapid, simple, and more importantly, convenient for the study and monitoring of other antigens or biocompounds.

* Address correspondence to this author. Phone/Fax: +86-23-6825-4000. E-mail: tdping@swu.edu.cn (D. Tang) or yuanruo@swu.edu.cn (R. Yuan).

10.1021/jp060950s CCC: $33.50
Published on Web 05/24/2006

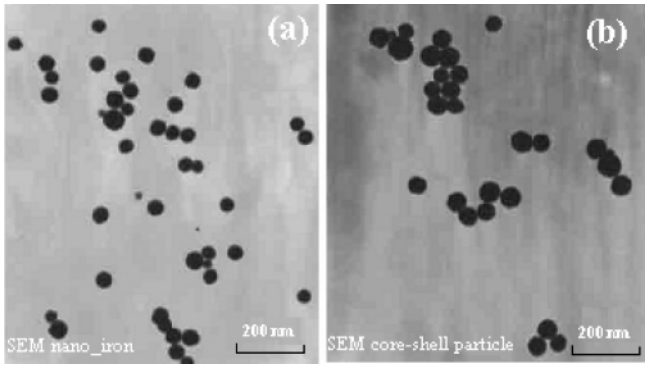

Figure 1. TEM images of pure Fe_3O_4 nanoparticles (a) and core−shell Fe_3O_4@Ag nanoparticles (b).

2. Experimental and Methods

2.1. Reagents. Carcinoembryonic antigen (CEA) and murine monoclonal carcinoembryonic antibody (anti-CEA) were purchased from Bosai Bioengin. Co. (Zhengzhou, China). Nafion and $AgNO_3$ were purchased from Sigma-Aldrich (USA). Carbon graphite powder (<325 mesh, Johnson Matthey) and paraffin oil (Fluka) were used for the preparation of carbon past electrode. Prior to the preparation, the graphite powder was treated at 700 °C for 30 s in a muffle furnace. All other chemicals were of analytical grade and were used as received. Phosphate buffer saline (PBS, pH 7.4) contained 137 mM NaCl, 2.7 mM KCl, 87 mM K_2HPO_4, and 14 mM KH_2PO_4. All solutions were made up with twice-distilled water. The serum samples were obtained from two clinically diagnosed patients with colorectal carcinomas. The sera were separated from the cell, without hemolysis.

2.2. Preparation of the Magnetic $(Fe_3O_4)_{core}-Ag_{shell}$ Nanoparitices (MNPs). Fe_3O_4 nanoparticles were prepared according to Massart's method.[28,29] The magnetic $(Fe_3O_4)_{core}-Ag_{shell}$ nanoparticles were prepared according to the literature[28,29] with a little modification. To coat the Fe_3O_4 particles with silver, five different sets (M_1, M_2, M_3, M_4, and M_5) were prepared, taking 0.5 g of glucose, Fe_3O_4 particles, and $AgNO_3$ solution, varying the proportion of Fe_3O_4 to Ag(I) ions in five different sets. The molar ratio of Fe_3O_4 to $AgNO_3$ was 1:0.1, 1:0.5, 1:1, 1:1.5, and 1:2 for the sets M_1, M_2, M_3, M_4, and M_5, respectively. All the sets were sonicated for 15 min and then they were heated in a water bath for 1 h with slow stirring. As the particles are gradually coated by silver, the black Fe_3O_4 particles turn brownish in color. These silver-coated particles were separated out from the solutions by centrifugation. After the particles were separated, the decanted supernatant liquid was fully transparent. The nanoparticle sizes were confirmed by transmission electron microscopy (TEM, H600, Hitachi Instrument Co., Japan), and the mean sizes were 40 and 46 nm for purified Fe_3O_4 nanoparticles and the $(Fe_3O_4)_{core}-Ag_{shell}$ nanoparticles, respectively (Figure 1).

2.3. Immobilization of Anti-CEA on the Magnetic $(Fe_3O_4)_{core}-Ag_{shell}$ Nanoparticle Surface (anti-CEA/Fe_3O_4@Ag). A self-assembly technique was adopted for immobilization of anti-CEA on the $(Fe_3O_4)_{core}-Ag_{shell}$ magnetic nanopariticle surface. Prior to the experiment, the $(Fe_3O_4)_{core}-Ag_{shell}$ magnetic nanoparticles were centrifugated and the precipitates were washed with pH 7.4 PBS three times. After adding 5 mL of PBS, 3 mL of anti-CEA was added, and the mixture was agitated for 24 h at 4 °C. Excess antibodies were removed by washing with pH 7.4 PBS; the anti-CEA/Fe_3O_4@Ag particles were stored at 4 °C when not in use.

2.4. Fabrication of the Immunosensors. The carbon paste electrodes (CPEs) were prepared by the following method (Scheme 1). Paraffin oil (1.2 mL) was added into 10 mg of graphite powder, and the resulting mixture was stirred thoroughly. A glass tube (10 mm in diameter and 20 mm in depth) was initially filled with a magnet (10 mm in diameter and 2 mm in depth, to produce an inhomogeneous magnetic density, 0.2 T at the surface), then a portion of the resulting paste was put into the glass tube with electrical contact; in the meantime, a copper wire was inserted into the back of the mixture. The obtained magnetic carbon paste electrodes (MCPEs) were dried and stored for a day at 4 °C. After the electrode tip was gently rubbed on a fine paper to produce a flat surface and cleaned with doubly distilled water, it was immersed in the Nafion ethanol solution (v/v, 1.5%) for 5 min at room temperature and then removed and parched with an infrared light for 20 min. Following that, the formed electrode was dipped into an anti-CEA modified $(Fe_3O_4)_{core}-Ag_{shell}$ magnetic nanoparticles suspension for 4 h at 4 °C. Finally, the obtained anti-CEA/Fe_3O_4@Ag/Nafion/MCPE was washed thoroughly with twice-distilled water and used for the following experiments.

2.5. Electrochemical Measurements. The conventional three-electrode setup was used for voltammetry and ac impedance experiments. The three-electrode system consisted of either MCPE or Nafion/MCPE, or Fe_3O_4@Ag/Nafion/MCPE, or anti-CEA/Fe_3O_4@Ag/Nafion/MCPE as the working electrode, a SCE reference electrode, and a platinum wire auxiliary electrode. An AutoLab electrochemical cell (Eco Chemie, The Netherlands) was employed in this study. The electrochemical behavior of the anti-CEA/Fe_3O_4@Ag/Nafion/MCPE electrode were studied with cyclic voltammetry (CV) in 10 mM $Fe(CN)_6^{4-/3-}$ solution in the potential range from 0.0 to +1.1 V at 50 mV·s^{-1}. The electrochemical impedances of the electrode were measured on a Model IM6e (ZAHNER Elektrick, Germany) at 10 discrete frequencies per decade from 0.01 Hz to 100 kHz with an amplitude of 5 mV (rms) in 10 mM $Fe(CN)_6^{4-/3-}$ solution. The acquired data were analyzed on the basis of equivalent electrical circuits by a nonlinear least-squares method. All the experiments were performed at 25 ± 0.5 °C.

Potentiometric measurements were performed by a digital ion analyzer (Model PHS-3C, Dazhong Instruments, Shanghai,

SCHEME 1: Schematic Illustration of the MCPE and the Anti-CEA/Fe_3O_4@Ag/Nafion/MCPE Immunosensor

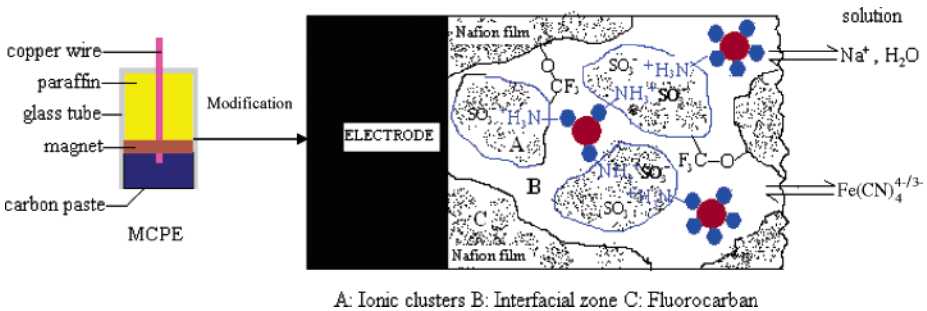

A: Ionic clusters B: Interfacial zone C: Fluorocarban

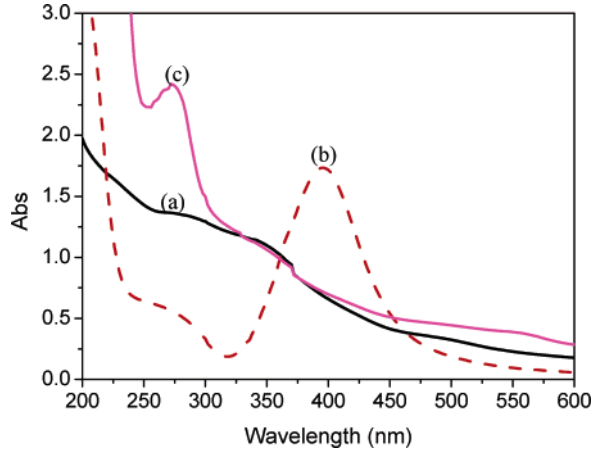

Figure 2. UV−vis absorption spectra of the Fe_3O_4 nanoparticles (a), the core−shell Fe_3O_4@Ag nanoparticles (b), and the anti-CEA/Fe_3O_4@Ag particles (c).

China). The principle of the electrochemical detection is based on the shift in the potential before and after the antigen−antibody reaction as the following equation: $\Delta E = E_1 - E_0$, where E_0 is the value of the steady-state potential (vs SCE) in a phosphate buffer solution (pH 7.4) before the antigen−antibody reaction and E_1 represents the value of the steady-state potential (vs SCE) after the antigen−antibody reaction under the same conditions.

The regeneration procedure of the immunosensors was performed by rinsing the sensor into 8 M urea for 5 min to break the antigen−antibody linkage while the regeneration of the electrode was carried out by turning the nut to extrude the paste layer and then polishing with a fine paper to produce a smooth shiny surface.

2.6. Fourier Transform Infrared Spectroscopic (FTIR) Characterization. Fourier transform infrared spectra were recorded on a Vector 22 FTIR spectrometer (Bruker) in a diffuse reflectance mode at a resolution of 4 cm^{-1}. Anti-CEA or anti-CEA-modified core−shell Fe_3O_4@Ag nanoparticles were deposited on a KBr tablet by droplet evaporation. Twenty scans were collected and averaged for each spectrum.

2.7. Atomic Force Microscopy (AFM) and UV−Vis Absorption Spectra. AFM measurements were performed with a digital Nanoscope IIIa multimode system (DI, Santa Barbara, CA). The images were acquired in the tapping mode. The AFM measurements were made in air at room temperature with the Si cantilever. The force constant of the cantilever was 01−0.6 N/m with the scan rate at 1−2 Hz. The UV−vis absorption spectra of the dispersions were measured by a UV−vis spectrometer (UV−vis 8500, Japan).

3. Results and Discussions

3.1. UV−Vis and AFM Analyses. The purity of the as-prepared magnetic Fe_3O_4@Ag nanoparticles was determined with UV−vis absorption spectrometry. The UV−vis absorption spectra of the dispersion of the present magnetic Fe_3O_4 nanoparticles are shown in Figure 2a. The Fe_3O_4 absorption spectra were complicated, and increased with the wavelength decrease in the range 570−200 nm, which is in agreement with the literature.[30] When Ag nanoparticles were deposited onto the Fe_3O_4 nanoparticle surface, 398 nm of the absorption peak was remarkably observed (Figure 2b), indicating that the $(Fe_3O_4)_{core}-Ag_{shell}$ nanoparticles have been formed by the deposition−precipitation method. Moreover, 278 nm of the absorption peak was obtained (Figure 2c) after anti-CEA was mixed with the $(Fe_3O_4)_{core}-Ag_{shell}$ particles solution for 4 h. The results indicate that anti-CEA molecules could be assembled onto the $(Fe_3O_4)_{core}-Ag_{shell}$ nanoparticle surface.

To further investigate the distribution of the anti-CEA/Fe_3O_4@Ag on the MCPE surface, AFM was used to obtain the dynamic images after each assembly step. Figure 3 shows the AFM images of differently modified MCPEs. As shown in Figure 3a, a three-dimensional network was observed on the Nafion-modified electrode surface, and the surface roughness ranged from 7 to 11 nm. Figure 3b reveals the broad distribution of anti-CEA/Fe_3O_4@Ag on the Nafion-modified electrode surface, and the surface roughness is wavy from 41 to 52 nm. In view of the fact that the diameter of the $(Fe_3O_4)_{core}-Ag_{shell}$ nanoparticles was 46 nm, anti-CEA/Fe_3O_4@Ag particles should be both diffused into the Nafion network and on the surface. On the basis of UV−vis and AFM results, we might make an inference that the anti-CEA/Fe_3O_4@Ag particles could be absorbed onto the MCPE surface.

3.2. FTIR Spectra of the Fe_3O_4@Ag and Anti-CEA/Fe_3O_4@Ag. The FTIR spectrum (Figure 4a) of pure Fe_3O_4 shows the stretching frequencies for the Fe−O bond at 423 and 572 cm^{-1}, which tally with the published results,[31] whereas for the silver-coated Fe_3O_4 the peak at 575 cm^{-1} shifted to 589 cm^{-1} and the peak at 423 cm^{-1} vanished completely (Figure 4b). This indicates the coating of Fe_3O_4 particles by silver again.

As is well-known, the shapes of the infrared absorption bands of amide I groups at 1610−1690 cm^{-1} corresponding to the C═O stretching vibration of peptide linkages and amide II groups around 1500−1600 cm^{-1} from a combination of N−H bending and C−N stretching can provide detailed information on the secondary structure of proteins.[32] When anti-CEA is mixed with the $(Fe_3O_4)_{core}-Ag_{shell}$ particles solution for 4 h, the FTIR spectrum of anti-CEA/Fe_3O_4@Ag particles shows two absorption peaks at 1650 and 1540 cm^{-1} (Figure 4c), which corresponded to the amide I and II groups of the proteins on anti-CEA. The weak bands occurring in the region of 1200−1400 cm^{-1} were assigned to the wagging and twisting vibrations of the $-CH_2$ group in these proteins and were commonly referred to as the progression bands,[33] suggesting that the anti-CEA, adsorbed on Fe_3O_4@Ag nanoparticles, retained their native characterizations. The slight deviation between absorption wavenumbers indicated an interaction between Fe_3O_4@Ag nanoparticles and anti-CEA.

3.3. Voltammetric Behavior of Anti-CEA/Fe_3O_4@Ag/Nafion/MCPE. No peak was observed at both MCPE and Nafion-modified MCPE in 10 mM $Fe(CN)_6^{4-/3-}$ solution (Figure 5a,b). The latter displayed a low background current (Figure 5b). The presence of Nafion resulted in a great decrease in the background current. The anti-CEA/Fe_3O_4@Ag modified Nafion/MCPE (anti-CEA/Fe_3O_4@Ag/Nafion/MCPE) exhibited a couple of weak redox peaks at 50 $mV \cdot s^{-1}$ (Figure 5c,d). The reason may be that the $(Fe_3O_4)_{core}-Ag_{shell}$ magnetic nanoparticles facilitate electron transfer. When the anti-CEA/Fe_3O_4@Ag particles were adsorbed on Nafion/MCPE with low magnetic density, anti-CEA/Fe_3O_4@Ag/Nafion/MCPE also showed a voltammetric response (Figure 5d). However, the cyclic voltammogram showed a lower current. The peak currents increased gradually with the increment of the magnetic density and reached a maximum value at 0.2 T. Further increase of the magnetic density led to decrease of the response signal, which was attributed to the increase of the resistance and double layer capacitance of the modified electrode. Moreover, the small magnetic density was favorable to minimize the interferences

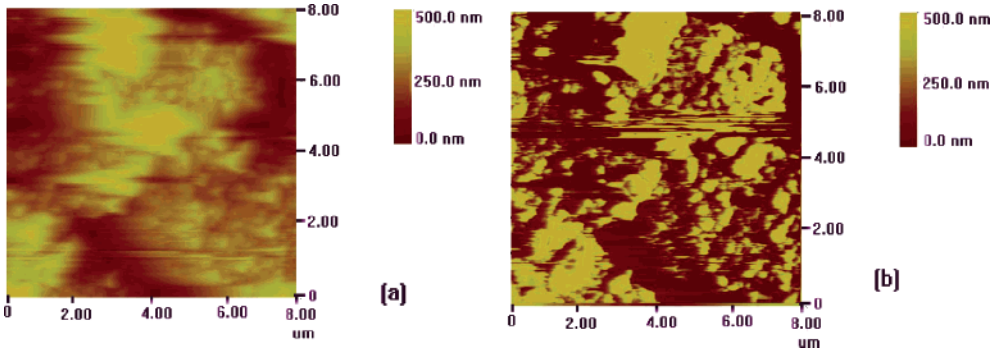

Figure 3. AFM images of the Nafion modified surface (a) and the anti-CEA/Fe_3O_4@Ag/Nafion modified surface (b).

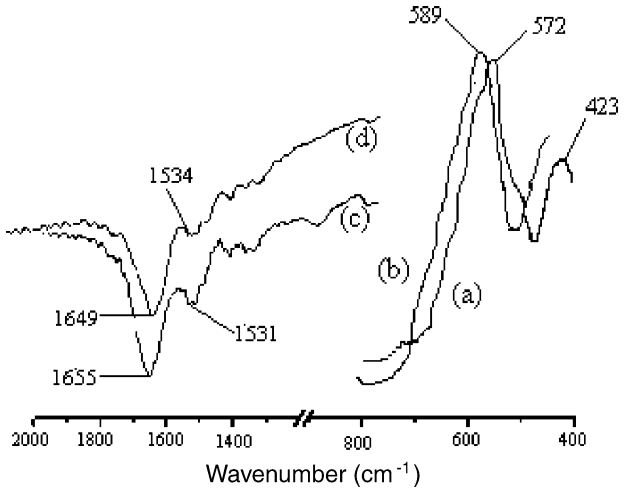

Figure 4. FTIR spectra of the magnetic Fe_3O_4 nanoparticles (a), the core−shell magnetic Fe_3O_4@Ag particles (b), the CEA antibody, (c) and the anti-CEA/Fe_3O_4@Ag composites (d).

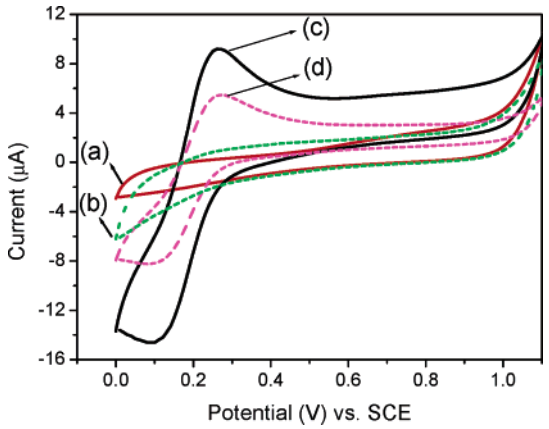

Figure 5. Cyclic voltammograms of MCPE (a), Nafion/MCPE (b), and anti-CEA/Fe_3O_4@Ag/Nafion/MCPE with different magnetic densities (c, d) in 10 mM $Fe(CN)_6^{4-/3-}$ solution. Scan rate: 50 mV·s^{-1}.

from the coexisting electroactive species. Therefore, 0.2 T of the magnetic density was chosen for the following experiments.

When the anti-CEA/Fe_3O_4@Ag/Nafion/MCPE immunosensor was stored at 4 °C and tested in pH 7.4 PBS everyday, the peak current decreased gradually. The storage time retaining 90% of its initial response was 6 days. Contrarily, the peak current of anti-CEA/Fe_3O_4@Ag/MCPE immunosensor showed a drastic drop. The reason may be that CEA antibody is a positively charged species in pH 7.4 PBS and it can easily assemble onto the Nafion surface as the Nafion is a good protonic conductor.

3.4. Direct Potentiometric Determination of CEA. In this study, the potential shifts before and after the antigen−antibody reaction were recorded by potentiometry. To arrive at the optimum conditions for CEA detection on anti-CEA/Fe_3O_4@Ag/Nafion/MCPE, both the electrode conditions and potentiometric response parameters must be optimized. As to the electrode conditions, the magnetic density (as described above) and the composition of the magnetic Fe_3O_4@Ag nanoparticles were considered. The Nafion weight percent in preparing the immunosensor was varied as another electrode parameter, and the maximum potential shift to the same CEA concentration was observed for a 1.5 wt % solution as shown in Figure 6a. An increase in Nafion weight percent obviously increases the film thickness and, thus, the ion-exchange capacity as Nafion is well-known to be a good protonic conductor. Herein, the effect of Nafion on the potentiometric response of the immunosensor may be attributed to the interfacial phenomenon, rather than a bulk one. So, a 1.5 wt % Nafion solution was used for the preparation of the immunosensor.

The effect of the molar weight ratio of Fe_3O_4 and $AgNO_3$ for the preparation of Ag@Fe_3O_4 nanoparticles on potentiometic responses of the immunosensor was also investigated between 1:0.1 and 1:2 in the presence of 20 ng·mL^{-1} of CEA. As can be seen in Figure 6b, the highest signal-to-background potential was obtained at 1:0.2. When the molar weight ratio of Fe_3O_4 and $AgNO_3$ was less than 1:0.2, a higher signal potential was achieved; however, the background potential also increased. Thus, a 1:0.2 molar weight ratio of Fe_3O_4 and $AgNO_3$ was selected for the preparation of Fe_3O_4@Ag nanoparticles.

Figure 7a shows a typical time response of the output voltage of the anti-CEA/Fe_3O_4@Ag/Nafion/MCPE in the absence and presence of CEA under the optimized experimental conditions in 0.1 M PBS (pH 7.4). In the absence of CEA, only low background potential was observed. Upon addition of CEA to the buffer solution, the output voltage increased rapidly with the elapse of time and converged after 3 min, which was due to increasing the electric charge density on the electrode surface after the antigen−antibody reaction.[34] Furthermore, this result indicates that the reaction between the immobilized anti-CEA and free CEA is an equilibrium process.

Figure 7b shows the calibration curve of the anti-CEA/Fe_3O_4@Ag/Nafion/MCPE to different CEA standard samples under optimal experimental conditions. The curve is not a linear one, as is commonly observed for immunoassays. A curve-fitting procedure could be used for the calibration procedure. A pseudolinear relationship between the potential and the logarithm of the concentration of CEA, however, can be fitted to the experimental points from 1.5 to 200 ng·mL^{-1}. The linear regression equation is ΔE (mV) = −6.3077 + 25.853 log $C_{[CEA]}$ (ng·mL^{-1}) with a detection limit of 0.5 ng·mL^{-1} (estimated to be 3 times the standard deviation of zero dose−response), which coincides with the lower bound of the pseudolinear part of the

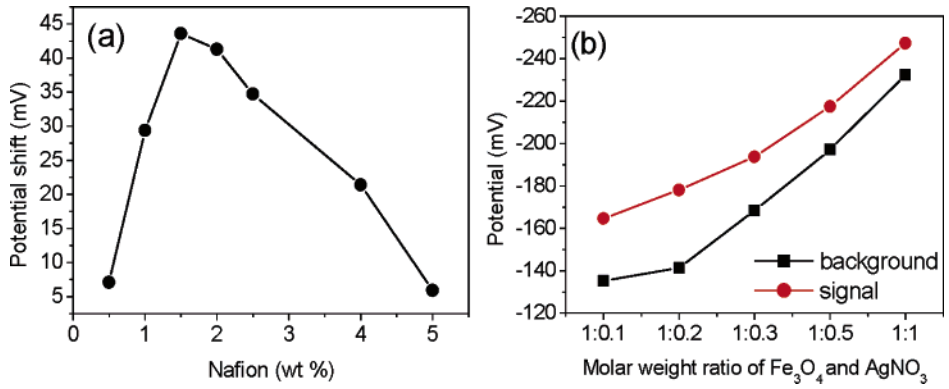

Figure 6. Effects of Nafion (a) and different molar ratios of Fe_3O_4 and $AgNO_3$ (b) on potentiometric responses of the immunosensor to the same concentration of CEA antigen.

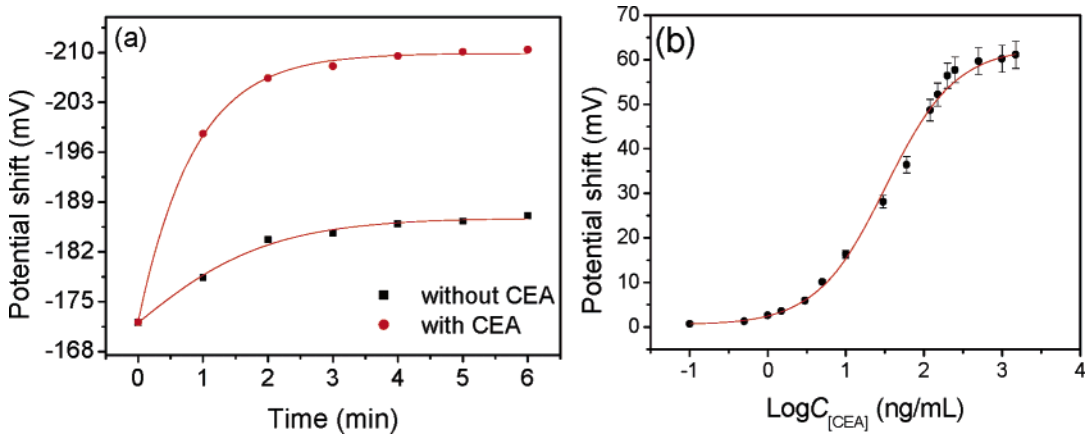

Figure 7. Relationship between potentiometric response (mV) and time (min) in the presence and absence of CEA (a) and the calibration curve to different CEA concentrations of anti-CEA/Fe_3O_4@Ag/Nafion/MCPE (b) in 0.1 M PBS (pH 7.4).

calibration curve. A relative standard deviation of 5.1% was obtained in the pseudolinear range after the corresponding incubation with four sensors. This indicates that the distribution of the anti-CEA in the bulk is uniform and that the anti-CEA/Fe_3O_4@Ag/Nafion/MCPE can offer reliable results for the quantitative determination of CEA. To characterize the reproducibility of the anti-CEA/Fe_3O_4@Ag/Nafion/MCPE, repetitive measurements/regeneration cycles were carried out at 4.9, 60, and 180 ng·mL^{-1} CEA, respectively. The reproducibility was excellent with results of six successive measurements that showed 1.3−4.1% coefficient of variation. When the immunosensor was not in use, it was stored in pH 7.4 PBS at 4 °C. No obvious change was observed after a 6-day storage.

3.5. Detection of Serum CEA Levels. The serum CEA levels in two samples were detected by using the proposed potentiometric immunosensor. As a result, the mean serum CEA concentrations obtained by the proposed CEA immunosensor were 32.5 and 41.3 ng·mL^{-1}, respectively, while the values measured by the standard ELISA were 37.5 and 47.3 ng·mL^{-1}, respectively. They were in acceptable agreement. The relative errors of the results acquired by two methods were 10.1% and 9.6%, respectively. Therefore, the developed immunoassay methodology could be satisfactorily applied to the clinical determination of the CEA level in humans.

3.6. Response Mechanism and Ac Impedance Analysis of the Immunosensors. As to potentiometric sensors, membrane potential mainly consists of surface potential (i.e., Donnan potential) and diffusion potential.[37] When the concentrations of electrolyte on both sides of the membrane are invariable, the sensitivity of the sensors depends on the charge density on membrane and the transferred number of ions. Either antibodies or antigens in aqueous solution have a net electrical charge polarity, which is correlated to the isoelectric points of the species and the ionic composition of the solution. If antibodies are immobilized on the electrode, the surface charge of the electrode will rely on the net charge of the immobilized antibody. When antigen molecules are present in the solution, the immunochemical reaction will take place at the interface with a resulting change of the surface charge. This change can be measured potentiometrically against the reference electrode immersed in the same solution.

Ac impedance spectroscopy is a rapidly developing electrochemical technique for the characterization of biomaterial-functionalized electrodes and biocatalytic transformations at electrode surface, and specifically for the transduction of biosening events at electrodes of film-effect transistor devices. In immunosensors, the formation of antigen−antibody complexes on conductive supports yields a chemically modified film on the surface that alters the impedance features of the interface. The composite perturbs the double-charged layer existing at the electrode/electrolyte interface resulting in the increase of its thickness, and the insulation of the electrode surface with respect to redox labels added to the solution. This results in the capacitance change and electron-transfer resistance change at the interface, respectively. Figure 8 shows the Nyquist diagrams of the anti-CEA/Fe_3O_4@Ag/Nafion/MCPE before and after the reaction with CEA in 10 mM $Fe(CN)_6^{4-/3-}$ solution. As was seen from Figure 8, there are two semicircles and one Warburg resistance. Moreover, the two semicircles increased with the increment of CEA concentration.

Figure 9 shows the generalized equivalent circuit and the Nyquist plot simulated for the equivalent circuit of anti-CEA/

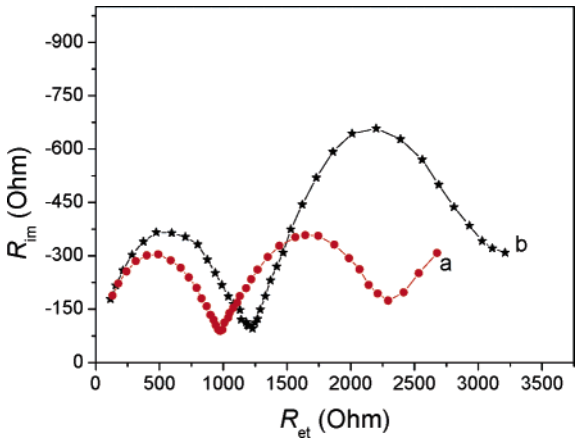

Figure 8. Faradaic impedance spectra of anti-CEA/Fe_3O_4@Ag/Nafion/MCPE in the absence (a) and presence (b) of CEA in 10 mM $Fe(CN)_6^{4-/3-}$ solution.

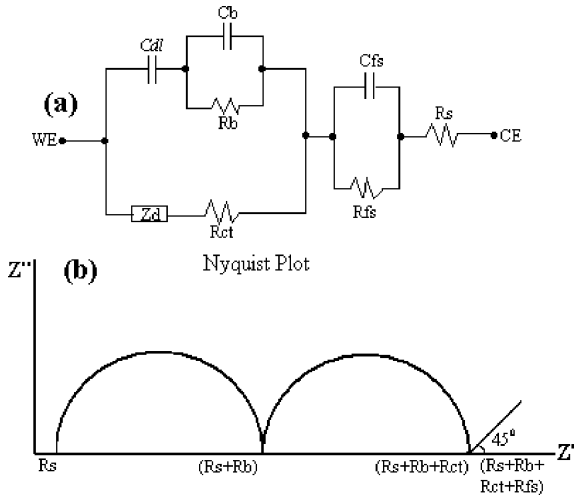

Figure 9. Equivalent circuit (a) and resulting impedance spectrum (b) of anti-CEA/Fe_3O_4@Ag/Nafion/MCPE. Physicochemical characteristics modeled by different components are specified in the text.

Fe_3O_4@Ag/Nafion/MCPE. The morphology of anti-CEA/Fe_3O_4@Ag/Nafion/MCPE, as shown in Scheme 1, is represented by hydrated SO_3^- headgroups and counterion clusters (zone A) are interconnected by short channels (zone B) immersed in a fluorocarbon backbone network (zone C). Because of the strongly hydrophobic backbone and highly hydrophilic terminal group, it is not surprising that some form of phase separation occurs in Nafion. The ac perturbation in the interface can be represented by a modified Randles equivalent circuit to accommodate the influences of the additional heterogeneous polymer phase.[35,36] The anti-CEA/Fe_3O_4@Ag/Nafion/MCPE interface is represented by the double-layer capacitance (C_{dl}) in parallel connection with a charge-transfer resistance (R_{ct}) (Figure 9a). Usually, the capacitance line in a Nyquist plot at a low frequency region inclined constantly by an angle between 0 and 45°. The deviation from vertical for an ideal capacitor is attributed to the dispersion of frequency due to the rough surface that is often associated with a solid electrode.[38] Z_d of Figure 9a represents the mass transport limitation through bulk polymer. The parallel combination of bulk resistance (R_b) and bulk capacitance (C_b) represents the bulk dielectric properties of Nafion. To maintain the electroneutrality with the Nafion film, the cations/anions extrude into the Nafion film. Thus, the circuit is accommodated by the inclusion of additional R_{fs} and C_{fs} in parallel combination. Finally, the circuit is terminated with the R_s in serial connection, representing the solution resistance and uncompensated drop.

In the Nyquist plot (Figure 9b), the first semicircle appearing at a very high frequency domain represents the dielectric properties of anti-CEA/Fe_3O_4@Ag/Nafion while the second semicircle arises due to the mass-transfer limitation of the redox $Fe(CN)_4^{4-/3-}$ that couples with a typical characteristic of 45° with respect to the Z' axis. At low-frequency domain, a vertical line is observed due to the capacitance of the film. Apart from Z_d, all other components in the circuit are assumed independent of frequency. When the anti-CEA/Fe_3O_4@Ag/Nafion/MCPE electrode reacted with CEA antigen, the diameters of these two semicircles were increased. This is believed to be the prime cause for the increase in the antigen−antibody complex coating the electrode surface after the anti-CEA-CEA reaction. According to the literature,[35,39] the semicircle in the higher frequency of the Nyquist plot increased at lower water contents and the conductivity of the Nafion film strongly depended on the water contents inside the film. For the lower water content, not only was the conductivity diminished but also the microstructure of the Nafion changed. So the observed increase of the semicircle with the increased CEA concentration in the present work is due to the uptakes of less H_2O and $Fe(CN)_4^{4-/3-}$. This led to the decreased uptake of $Fe(CN)_4^{4-/3-}$ inside the MCPE. Moreover, the bulk capacitance also decreased with the increment of CEA concentration, indicating that fewer ionic clusters result at higher CEA concentration. Thus, the impedance of the first semicircle was increased after the antigen−antibody reaction. Furthermore, the complex was coated on the Nafion-modified MCPE surface and acted as an inert electron layer, hindering the $Fe(CN)_4^{4-/3-}$ toward the MCPE surface. Also, the diameter of the second semicircle was also increased after the CEA antibody reacted with CEA antigen.

4. Conclusions

This work introduces the advantageous features of carbon paste technology with core−shell magnetic Fe_3O_4@Ag nanoparticle materials to construct a nontoxic biomimetic interface and develop a novel immobilization method for proteins. The immobilized anti-CEA molecules exhibit an excellent electrochemical response selective to the CEA in pH 7.4 PBS. Hopefully, the immobilized technique and the detection methodology can be further developed for other proteins, such as enzyme, DNA, tissue, and living tumor cell.

Acknowledgment. This work was supported by the NNSF of China (29705001), the Chinese Education Ministry Foundation for Excellent Younger Teachers (No. 2002-40), and the Natural Science Foundation of Chongqing City (No. 20027477), China.

References and Notes

(1) Benchimol, S.; Fuks, A.; Jothy, S.; Beauchemin, N.; Shirota, K.; Stanners, C. P. *Cell* **1989**, *57*, 327−334.
(2) Oikawa, S.; Inuzuka, C.; Kuroki, M.; Matsuoka, Y.; Kosaki, G.; Nakazato, H. *Biochem. Biophys. Res. Commun.* **1989**, *164*, 39−45.
(3) Goldenberg, D. M.; Sharkey, R. M.; Primus, F. J. *J. Natl. Cancer Inst.* **1976**, *57*, 11−22.
(4) Tang, D. P.; Yuan, R.; Chai, Y.; Zhong, X.; Liu, Y.; Dai, J. *Biochem. Eng. J.* **2004**, *22*, 43−49.
(5) Tang, D. P.; Yuan, R.; Chai, Y.; Zhong, X.; Liu, Y.; Dai, J. *Langmuir* **2004**, *20*, 7240−7245.
(6) Wang, H.; Li, J.; Ding, Y.; Lei, C.; Shen, G. L.; Yu, R. Q. *Biosens. Bioelectron.* **2004**, *19*, 701−709.
(7) Tang, D. P.; Yuan, R.; Chai, Y.; Zhong, X.; Liu, Y.; Dai, J. *Anal. Biochem.* **2004**, *333*, 345−350.
(8) Tang, D. P.; Yuan, R.; Chai, Y.; Zhong, X.; Liu, Y.; Dai, J. *Anal. Bioanal. Chem.* **2005**, *381*, 674−680.
(9) Fu, Y. Z.; Yuan, R.; Tang, D. P.; Chai, Y. Q.; Xu, L. *Colloids Surf. B* **2005**, *40*, 61−66.

(10) Du, D.; Yan, F.; Liu, S. L.; Ju, H. X. *J. Immunol. Methods* **2003**, *283*, 67−75.
(11) Ye, Y. K.; Zhao, J. H.; Yan, F.; Zhu, Y. L.; Ju, H. X. *Biosens. Bioelectron.* **2003**, *18*, 1501−1508.
(12) Zhuo, Y.; Yuan, R.; Chai, Y. Q.; Tang, D. P.; Zhang, Y.; Wang, N.; Li, X.; Zhu, Q. *Electrochem. Commun.* **2005**, *7*, 355−360.
(13) D'Souza, S. F. *Biosens. Bioelectron.* **2001**, *16*, 337−353.
(14) Du, D.; Liu, S.; Chen, J.; Ju, H.; Lian, H.; Li, J. *Biomaterials* **2005**, *26*, 6487−6495.
(15) SivaRaman, H.; Rao, S. B.; Pundle, A. V.; SivaRaman, C. *Biotechnol. Lett.* **1982**, *4*, 359−364.
(16) Miranda, C.; D'Souza, S. F. J. *Microbiol. Biotechnol.* **1988**, *3*, 60−65.
(17) Liu, S. Q.; Leech, D.; Ju, H. X. *Anal. Lett.* **2003**, *36*, 1−19.
(18) Gupta, A. K.; Curtis, A. S. G. *Biomaterials* **2004**, *25*, 3029−3240.
(19) Pankhurst, Q. A.; Connolly, J.; Jones, S. K. *J. Phys. D*: *Appl. Phys.* **2003**, *36*, R167−181.
(20) Wang, Y. X.; Hussain, S. M.; Krestin, G. P. *Eur. Radiol.* **2001**, *11*, 2319−2331.
(21) Lin, J.; Zhou, W.; Kumbhar, A.; Fang, J.; Carpenter, E. E.; O'Connor, C. J. *J. Solid State Chem.* **2001**, *159*, 26−31.
(22) Xu, H. K.; Sorensen, C. M.; Klabunde, K. J.; Hadjipanayis, G. C. *J. Mater. Reson.* **1992**, *7*, 712−716.
(23) Tartaj, P.; Gonzalez-Carreno, T.; Serna, C. J. *Langmuir* **2002**, *18*, 4556−4558.
(24) Tartaj, P.; Gonzalez-Carreno, T.; Serna, C. J. *Adv. Mater.* **2001**, *13*, 1620−1624.
(25) Santra, S.; Tapec, R.; Theodoropoulou, N.; Dobson, J.; Hebard, A.; Tan, W. *Langmuir* **2001**, *17*, 2900−2906.
(26) Mulvaney, P. *Langmuir* **1996**, *12*, 788−800.
(27) Link, S.; Wang, Z. L.; El-Sayed, M. A. *J. Phys. Chem. B* **1999**, *103*, 3529−3533.
(28) Mandal, M.; Kundu, S.; Ghosh, S.; Panigrahi, S.; Sau, T.; Yusuf, S.; Pal, T. *J. Colloid Interface Sci.* **2005**, *286*, 187−94.
(29) Tourinho, F. A.; Franck, R.; Massart, R. *J. Mater. Sci.* **1990**, *25*, 3249−3254.
(30) Chen, M.; Yang, P. *Harbin Gongcheng Daxue Xuebao* **2002**, *23*, 139−141.
(31) Cornell, R. M.; Schwertmann, U. *The Iron Oxides*: *Structure, Properties, Reactions, Occurrence and Uses*, VCH: New York, 1996; Vol. 134.
(32) Jackson, M.; Choo, L. P.; Watson, P. H. *Biochim. Biophys. Acta* **1995**, *1270*, 1−6.
(33) Dong, S.; Luo, G. A.; Feng, J.; Li, Q. W.; Gao, H. *Electroanalysis* **2001**, *13*, 30−33.
(34) Feng, C. L.; Xu, Y. H.; Song, L. M. *Sens. Actuators* **2000**, *66*, 190−192.
(35) Katz, E.; Willner, I. *Electroanalysis* **2003**, *1*, 913−947.
(36) Randles, J. E. B. *Discuss. Faraday Soc.* **1947**, *1*, 11−19.
(37) Aizawa, M. *Philos. Trans. R. Soc. London, Ser. B* **1987**, *316*, 121−134.
(38) Piela, B.; Wrons, P. K. *J. Electroanal. Chem.* **1995**, *388*, 69−79.
(39) Poucelly, G.; Oikonomou, A.; Gavach, C.; Hurwitz, H. D. *J. Electroanal. Chem.* **1990**, *287*, 43−59.